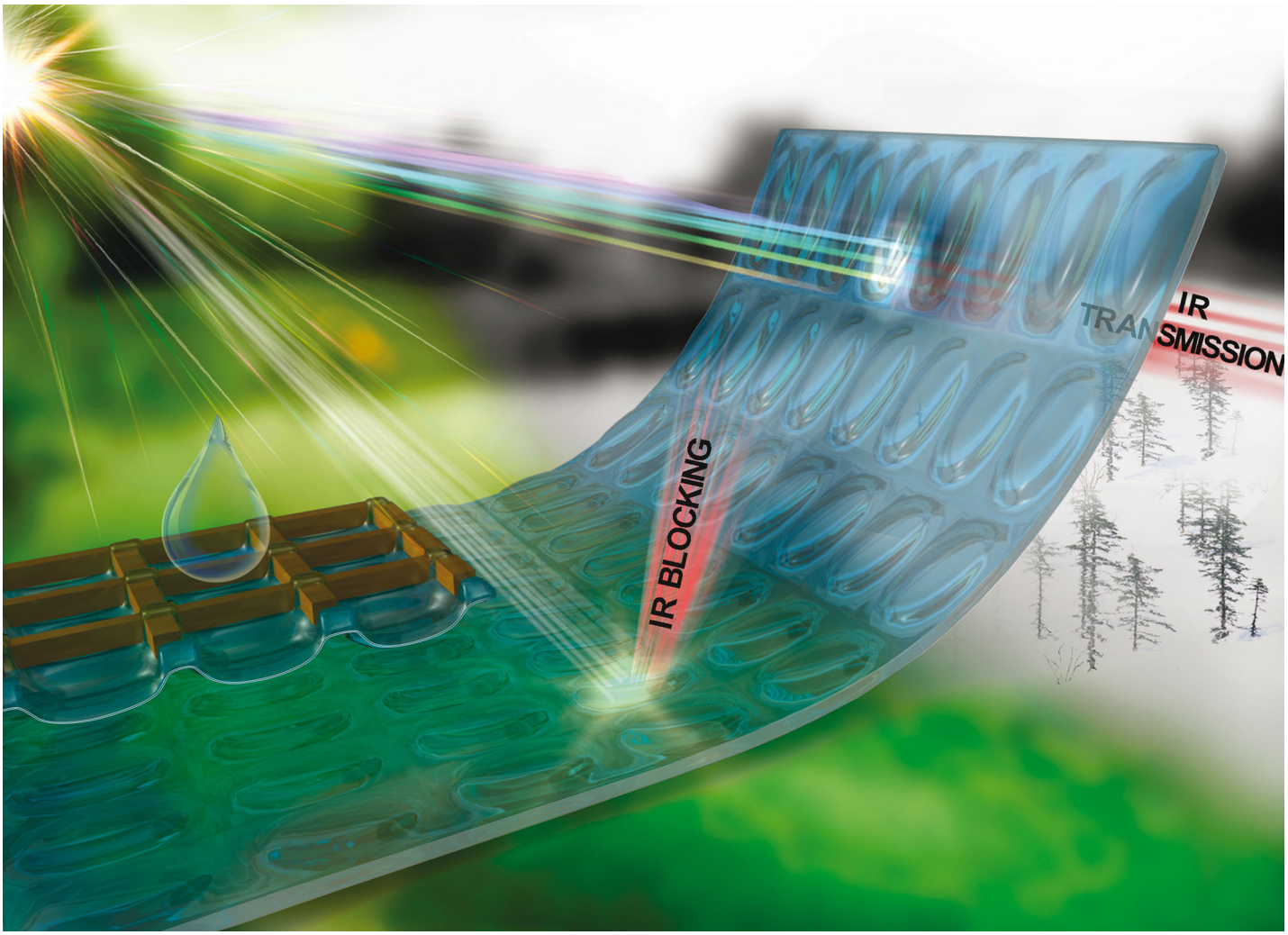


**Showcasing a study on micro-patterned vanadium dioxide thermochromic windows by Dr Yi Long at School of Materials Science and Engineering, Nanyang Technological University, and Prof. Shlomo Magdassi and Prof. Daniel Mandler at Institute of Chemistry, The Hebrew University.**

Periodic micro-patterned $VO_2$ thermochromic films by mesh printing

Facile meshing printing is employed to fabricate periodic micro-patterned structures of vanadium dioxide. Such structure is able to favorably transmit visible light without sacrificing large near-infrared modulation, with overall enhanced thermochromic properties.

## As featured in:


See Shlomo Magdassi, Daniel Mandler, Yi Long *et al.*, *J. Mater. Chem. C*, 2016, **4**, 8385.

ROYAL SOCIETY OF CHEMISTRY

www.rsc.org/MaterialsC

Registered charity number: 207890

Journal of Materials Chemistry C

PAPER

View Article Online
View Journal | View Issue



Cite this: J. Mater. Chem. C, 2016, 4, 8385

# Periodic micro-patterned $VO_2$ thermochromic films by mesh printing†

Qi Lu,[a] Chang Liu,[a] Ning Wang,[a] Shlomo Magdassi,*[b] Daniel Mandler*[b] and Yi Long*[a]

Received 29th June 2016,
Accepted 11th July 2016

DOI: 10.1039/c6tc02694j

www.rsc.org/MaterialsC

$VO_2$ has garnered much attention in recent years as a promising candidate for thermochromic window applications due to rising awareness about energy conservation. However, the trade-off between improving the luminous transmittance ($T_{lum}$) and solar modulation ability ($\Delta T_{sol}$) limits the commercialization of $VO_2$-based smart windows. Four major nanostructuring approaches were implemented to enhance both $T_{lum}$ and $\Delta T_{sol}$, namely nanocomposites, nanoporous films, biomimetic moth-eye structures and anti-reflection coating (ARC) multilayers. This work demonstrates a novel approach that fabricates periodic, micro-patterned structures of $VO_2$ using a facile screen printing method. The micro-patterned structure is able to favorably transmit visible light without sacrificing high near-infrared modulation, and the patterned film shows improved $T_{lum}$ (67% *vs.* 60%) and $\Delta T_{sol}$ (8.8% *vs.* 6.9%) compared with continuous films. By varying the thickness, periodicity and solid concentration, this approach can give a $\Delta T_{sol}$ of 14.9% combined with a $T_{lum}$ of 43.3%, which is comparable, if not superior to, some of the best reported results found using other approaches.

## Introduction

20 to 40 percent of energy consumption in developed countries can be attributed to buildings, and 10 to 20 percent of the primary energy usage of buildings account for heating or cooling purposes.[1,2] This provides a strong impetus for novel energy-saving solutions, and in particular, building-facade solutions have become increasingly popular. Thermochromic films are the most cost-effective chromogenic material as they exhibit an automatic change in solar transmission with changes in temperature.[3] Vanadium dioxide ($VO_2$) is one of the leading thermochromic materials.[4–6] Below the critical temperature of $\tau_c$ = 68 °C, $VO_2$ is in the monoclinic phase and is transparent to infrared light. As it transforms into a metallic tetragonal structure at $T > \tau_c$, it becomes highly absorbent of IR radiation.[7–9] Ideally, thermochromic coatings should have both high luminous transmittance ($T_{lum}$) and solar modulation ability ($\Delta T_{sol}$), but $VO_2$'s inherently high luminous absorption in both states renders it challenging to simultaneously increase $T_{lum}$ and $\Delta T_{sol}$. Most conventional $VO_2$ single layer films are able to achieve a $T_{lum}$ around 50% with a $\Delta T_{sol}$ of 5%.[10] Many endeavors to improve the performance of $VO_2$ based films have been attempted,[11] employing doping,[10,12–18] anti-reflection coating,[19] nanoporous structuring,[20,21] nanoparticle-based composites,[22–26] biomimetic nanostructuring,[27,28] organic materials,[29] and hybridization[30] as means to enhance both $T_{lum}$ and $\Delta T_{sol}$.

Liu Chang *et al.*[31] proposed the first finite difference time domain (FDTD) simulation work on nano-gridded, $VO_2$-based perforated films. The nano-sized opening would improve the transmission of short-wavelength visible light, while the abundant volume of $VO_2$ retained in the pattern maintains the film's good long-wavelength near-infrared (NIR) modulation abilities. The best-performing theoretical combination of 79% $T_{lum}$ and 14% $\Delta T_{sol}$ surpasses other theoretical work such as biomimetic nanostructuring,[28] nanothermochromism,[32] and nanoporous structuring.[33]

We report, for the first time, a micro-gridded structure inspired by Liu's design. It was fabricated using screen printing meshes with controlled film thickness, concentration and periodicity. Such structures could improve both $T_{lum}$ and $\Delta T_{sol}$ simultaneously, thus opening a new research direction in thermochromic $VO_2$ studies.

### Materials and equipment

$VO_2$ nanoparticles (Jingcheng Chemicals, China), dipropylene glycol methyl ether (DPM, 4.5 wt%), Disperbyk 180, and silica aluminum gel were used without further purification. Deionized water (18.2 MΩ) was used throughout the experiments.

[a] School of Materials Science and Engineering, Nanyang Technological University, 50 Nanyang Avenue, Singapore 639798. E-mail: longyi@ntu.edu.sg; Fax: +65 67911604; Tel: +65 67904599
[b] Institute of Chemistry, The Hebrew University, Edmond Safra Campus, Jerusalem 91904, Israel. E-mail: magdassi@mail.huji.ac.il, daniel.mandler@mail.huji.ac.il

† Electronic supplementary information (ESI) available. See DOI: 10.1039/c6tc02694j

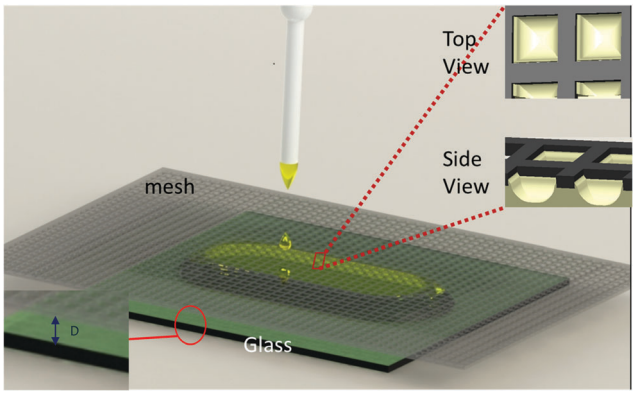


Fig. 1 The mesh is mounted on top of a glass substrate with a distance *D*. $VO_2$ is dispersed onto the glass pane using a pipette, whereby it immediately spreads across the mesh thread upon contact due to capillary forces. Inset: Enlarged picture of top view and side view showing the contact between the mesh and solution.

A $VO_2$/Si–Al gel mixture was prepared as reported,[4] which serves to provide structural support to the $VO_2$ grid films upon drying. 5 wt% mg of the filtered colloid was diluted to 0.5 wt%, 0.25 wt%, 0.167 wt% and 0.125 wt% with Si–Al gel. The solution was then vortexed and sonicated for 15 minutes for better dispersion and homogeneity.[34]

A soda glass substrate was sonicated with deionized water, followed by 95% ethanol solution, and finally with deionized water again for cleaning. The glass slide was dried in a furnace set at 100 °C. As illustrated in Fig. 1, the glass substrate was placed at the center of a hot plate. The screen printing mesh (Ponger 2000, Israel) was mounted directly above the glass substrate, and the vertical distance, *D*, between the bottom of the mesh and the top surface of the glass substrate, was carefully controlled. Using a 100 μL pipette, the $VO_2$/Si–Al gel mixture was applied onto the glass substrate through the meshes. When the nanoparticle (NP) dispersion was placed on top of the mesh (Fig. 1), upon contact, the liquid immediately wetted the mesh walls and filled up the space between the mesh and the glass substrate, resulting in the alignment of the NPs along the threads of the mesh (Fig. 1 inset side view). The substrate was heated at 50 °C for 12 hours to evaporate water from the matrix. Upon removal of the mesh, a periodic, waffle textured $VO_2$ film was formed (Fig. 1 inset top view).

### Characterization

The morphology and the SAED (selected area electron diffraction) of the purchased $VO_2$ nanoparticles were characterized using a transmission electron microscope (JEM-2010, JEOL, Japan) with an accelerating voltage of 200 kV.

The transmittance spectrum from 250 to 2500 nm was analysed using a UV-Vis-NIR spectrometer (Cary 5000, Agilent, USA) at normal incidence. A heating stage (PE120, Linkam, UK) was employed to control the temperature of the samples mounted on the spectrophotometer.

The sample films' morphology was studied using a field emission scanning electron microscope (JEM-7600F, JEOL, Japan) with an accelerating voltage of 5 kV.

The following equation was employed in the calculation of the film's performance in terms of its luminous transmittance (380–780 nm), IR transmittance (780–2500 nm), and solar transmittance, $T_{sol}$ (250–2500 nm):

$$T_{lum/IR/sol} = \frac{\int \varphi_{lum/IR/sol}(\lambda) T(\lambda) d\lambda}{\int \varphi_{lum/IR/sol}(\lambda) d\lambda} \quad (1)$$

where $T(\lambda)$ refers to the spectral transmittance and $\varphi_{lum}$ is the standard luminous efficiency function of photopic vision at the corresponding wavelength.[36] $\varphi_{IR}$ and $\varphi_{sol}$ denote the IR/solar irradiance spectrum distribution for air mass 1.5 (which corresponds to the sun standing at 37° above the horizon with 1.5 atmosphere thickness,[37] and in the presence of a solar zenith angle of 48.2°). $\Delta T_{lum/IR/sol}$ is obtained as the difference between $\Delta T_{lum/IR/sol}$ at 20 °C and $\Delta T_{lum/IR/sol}$ at 90 °C.

## Results and discussion

### Effects of thickness on optical properties

The particle size of the starting $VO_2$ powders is less than 100 nm with an oval shape and a uniform size distribution, as shown in Fig. 2a. The selected area electron diffraction (SAED) pattern (inset Fig. 2a) suggests the high purity of the polycrystalline $VO_2$ NPs. The thickness of the samples fabricated has been varied according to Fig. 1, using a mesh of size 325 μm. As shown in Fig. 2, grooved lines can be seen in places where mesh threads had come in contact with the film. Formation of the grooves under the threads can be attributed to surface tension, which attracts the solution towards the walls of the threads. The strong adhesion to the mesh threads draws the solution from the centre of each period, leading to the formation of a concave crater upon drying. SEM images illustrate the changes to the structure as the thickness *D* varies. When the thickness is low ($D$ = 0 μm) (Fig. 2b), a grid-like structure is produced with the main $VO_2$ content concentrated on both sides of the mesh threads. An increase in the thickness of film is observed to reduce the size of the crater and allows more solution to remain at the centre. The thickness of the film formed at the bottom of the crater also increases (Fig. 2c). In this case, the film is no longer a hollow grid; it forms a cone textured structure with periodically alternating crests and troughs. The cross-section view of the samples is shown in Fig. 2d and e. The increase in the thickness does not afford the formation of the patterned structure, albeit the film starts to adopt a waffle-like structure instead of a gridded structure when the thickness becomes greater.

As illustrated in Fig. 2f, increasing thickness (*D*) results in a gradual decrease in the transmittance in samples prepared with 0.25 wt% $VO_2$ dispersions at all wavelengths (250–2500 nm) at 90 °C. This is also observed in the visible range (380–780 nm) at 20 °C, thus accounting for decreasing averaged $T_{lum}$ as shown in Fig. 2g. A similar trend was observed for 0.5 wt% samples. The reduction in $T_{lum}$ is attributed to greater solar absorption due to the increased $VO_2$ content. However, such thickness–transmission correlation was not observed in the IR range (780–2500 nm) at 20 °C, as the 400 μm size sample gives the highest IR transmission. This is

 

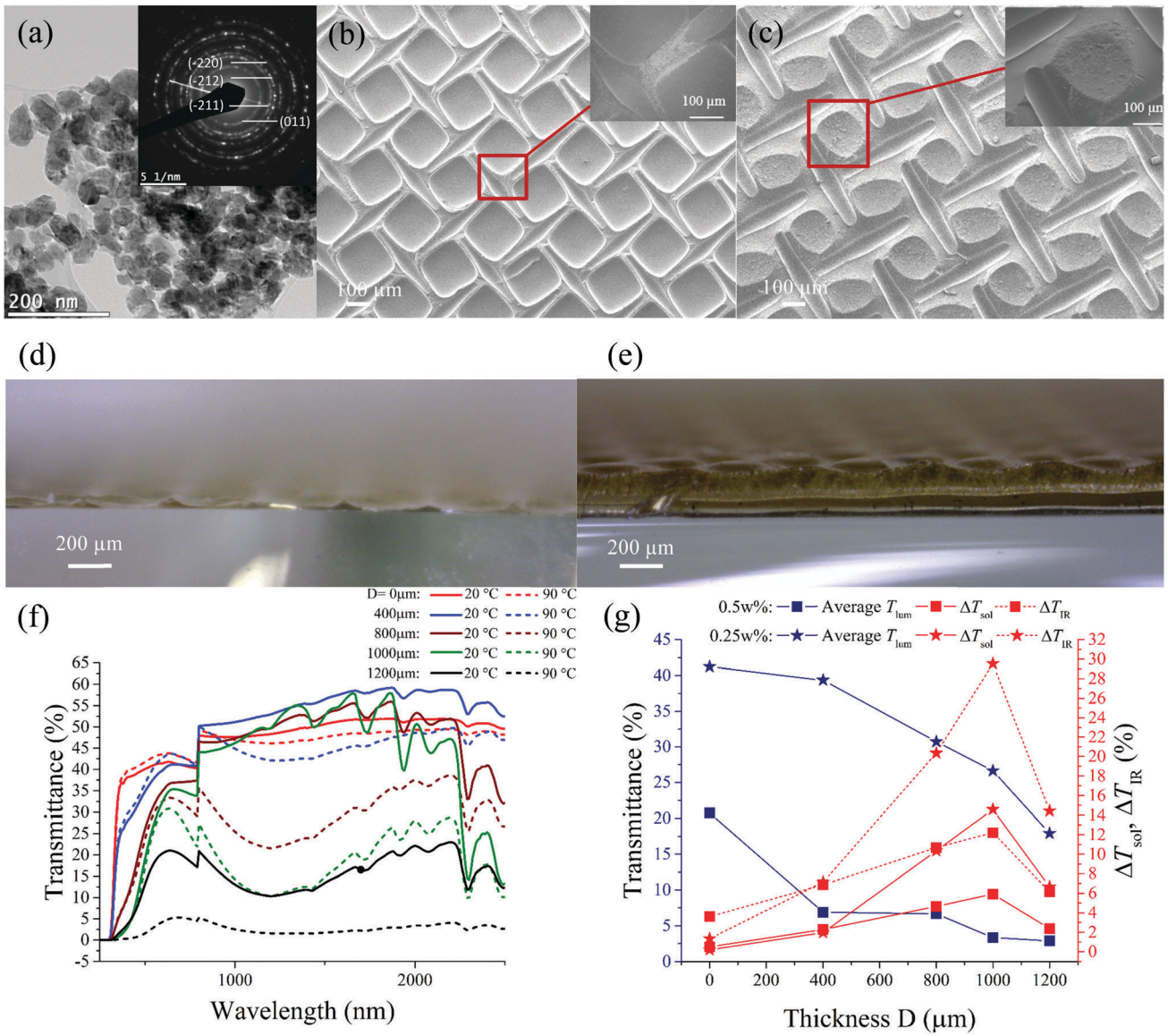


Fig. 2 Effects of thickness on film performance. (a) TEM images show the $VO_2$ powder to have good crystallinity with a uniform size; SEM image illustrates a film prepared using (b) $D$ = 0 μm and (c) $D$ = 1000 μm; optical image of the cross sectional view of the sample with (d) $D$ = 0 μm and (e) $D$ = 1000 μm (f) UV-Vis-NIR transmission for films with different thicknesses by adjusting the mesh glass distance; (g) thickness effects on $T_{lum}$, $\Delta T_{sol}$ and $\Delta T_{IR}$.

reflected by the trend in the IR contrast ($\Delta T_{IR}$), which increases with thickness up to 1000 μm. Enhanced $\Delta T_{IR}$ is correlated with higher $\Delta T_{sol}$ for both concentrations because large portions of $\Delta T_{sol}$ come from the IR contrast. $\Delta T_{sol}$ starts to decrease when the thickness increases to 1200 μm, and such thickness/performance correlation was predicted by Liu Chang *et al.*,[31] who suggested that a grid-design will enhance $\Delta T_{sol}$ up to a certain thickness before it becomes a static absorber with much reduced contrast. It is worth noting that the satellite peaks in the 1000 to 2500 nm range (Fig. 2f) are due to the pure Si–Al gel matrix as shown in Fig. S1 (ESI†).

### $VO_2$ concentration effect

By fixing the distance $D$ to 1000 μm, the performance of different $VO_2$ content ranging from 0.125 to 0.5 wt% was investigated. The varying $VO_2$ content results in different solution properties, thereby changing the surface morphology of the patterned films. By changing the concentration from 0.25 wt% to the 0.5 wt%, as shown in Fig. 3a and b, we observe increasing aggregation of $VO_2$ towards the center, and the groove formed under the thread of the mesh starts to become more uniform and well defined. Fig. 3c and d illustrate the real samples prepared using the aforementioned concentrations. The 0.5 wt% sample appears darker than the 0.25 wt% sample, indicating the higher solid concentration.

As illustrated in Fig. 3e, the concentration has an inverse correlation with transmittance. Samples prepared with $D$ = 1000 μm experience a drop in transmittance in the visible spectrum (380–780 nm) at both 20 °C and 90 °C as the

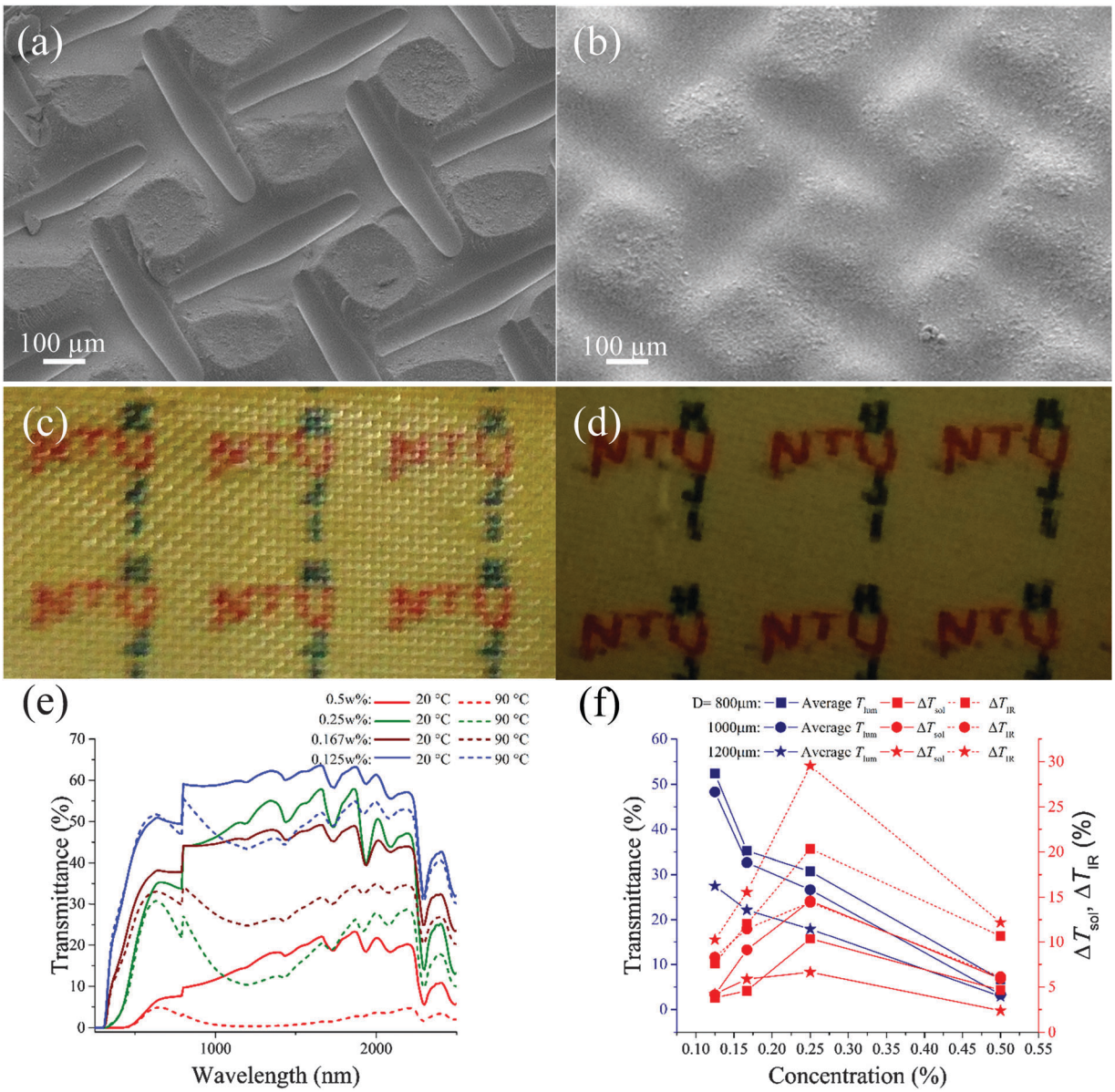


Fig. 3 Effect of $VO_2$ concentration of film: SEM image of film prepared with (a) 0.25 wt% (b) 0.5 wt% dispersion. Pictures taken of samples with (c) 0.25 wt% concentration and (d) 0.5 wt% concentration; (e) UV-Vis-NIR transmission for 1000 μm samples with 0.25 wt% to 0.5 wt% (f) the concentration effects on $T_{lum}$, $\Delta T_{sol}$ and $\Delta T_{IR}$.

concentration increases. This corroborates with the observation that the average $T_{lum}$ depreciates with rising concentration. The same trend is not observed in the IR spectrum (780–2500 nm) at 20 °C, with the 0.25 wt% sample having a higher transmittance. This accounts for the highest $\Delta T_{IR}$ displayed by the 0.25 wt% sample, as $\Delta T_{IR}$ is the difference in transmittance in the IR range at the two temperatures. As $\Delta T_{IR}$ accounts for a large portion of solar contrast, higher $\Delta T_{IR}$ leads to higher $\Delta T_{sol}$, as observed in Fig. 3f for both distances $D$. The increasing trend in both $\Delta T_{sol}$ and $\Delta T_{IR}$ does not continue indefinitely. They both peak at 0.25 wt% concentration and decrease when the concentration is higher.[31] This could be accounted for by excessive absorption in both states, which suggests that an optimal design requires one to avoid excessively concentrated dispersions.

### Effect of mesh periodicity

The SEM image (Fig. 4a–c) shows that a smaller mesh opening size results in a smaller center crater size. Meanwhile, the groove under each mesh thread becomes more pronounced compared with a larger mesh opening. Fig. 4d–f illustrate the real samples prepared. The reduction in the mesh size results in less pronounced gridded structures on the surface of the films formed.

As shown in Fig. 4g, samples prepared with $D$ = 1000 μm and a concentration of 0.5 wt% have higher transmittance in the

 

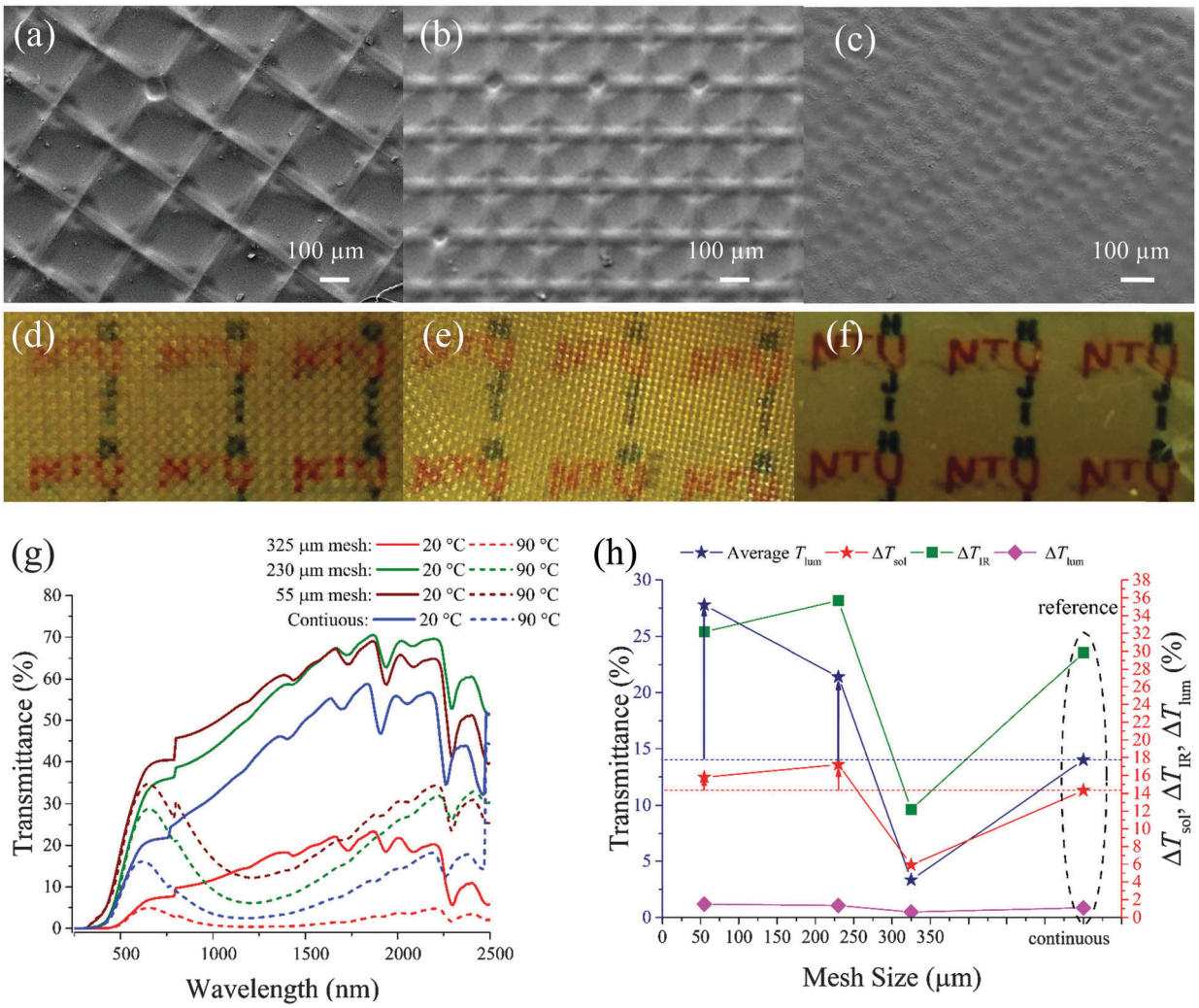


Fig. 4 Effect of the mesh opening size (periodicity) on film performance. SEM image of film prepared using (a) 325 μm, (b) 230 μm, and (c) 55 μm mesh. Real samples as shown in (d) 325 μm, (e) 230 μm, and (f) 55 μm. (g) UV-Vis-NIR transmission for $D$ = 1000 μm films prepared with 0.5 wt% $VO_2$ dispersion; (h) mesh size effects on $\Delta T_{sol}$, $\Delta T_{IR}$, and $\Delta T_{lum}$.

visible spectrum (380–780 nm) at both 20 and 90 °C when a smaller mesh periodicity is used, and this trend is consistent with the theoretical calculation.[31] The 325 μm mesh sample produces inferior results even compared to continuous samples due to low transmittance in both the luminous and IR ranges in both states. Indeed, the highest average $T_{lum}$ is produced using a mesh opening of 55 μm. In contrast to $\Delta T_{lum}$, $\Delta T_{IR}$ is very sensitive to the change of mesh periodicity as shown in Fig. 4h, and the high $\Delta T_{IR}$ results in a corresponding change in $\Delta T_{sol}$. Compared with the continuous sample, both the 230 and 55 μm mesh samples show much higher transmittance in the entire spectrum in both states with higher average $T_{lum}$ and more importantly $\Delta T_{sol}$. It is interesting to note that the 230-mesh size sample can obtain $T_{lum}$ of 21.4% with a $\Delta T_{sol}$ as high as 17.2%. This exceeds the highest reported $\Delta T_{sol}$ of 16.5% coupled with a poor $T_{lum}$ of 10.5%, as predicted by theoretical calculation.[31] This is due to the fact that the simulation is based on a perforated continuous $VO_2$ film while nanocomposite $VO_2$ is used in this project to form such a periodic gridded structure. A similar trend is also observed in the 0.25 wt% samples (Fig. S2, ESI†). Both the 230 and 55 μm mesh samples show much higher transmittance over the entire spectrum in both states with higher average $T_{lum}$ compared with the continuous sample.

## Optimization of performance

Previous discussions have established the importance of $VO_2$ concentration, thickness, and mesh size (periodicity) for the optical properties of the film. Generally, a higher concentration has been shown to increase the solar modulation ability due to the increased $VO_2$ content, albeit with the inevitable trade-off with luminous transmittance. Meanwhile, increasing the thickness further enhances $\Delta T_{sol}$, but only to a maximum thickness of $D$ = 1000 μm, as further thickening would result in excessive absorption of incident rays and, therefore, degrade the performance. Finally, a smaller mesh size offers a significantly higher $T_{lum}$.

Therefore, we set $D$ to 1000 μm and prepared samples using 230 and 55 μm meshes since both were proven to offer better

Table 1 Optimized thermochromic properties with a fixed thickness (1000 μm) and concentration (0.25 wt%) with two different mesh sizes 230 and 55 μm

| Mesh (μm) | Ave. $T_{lum}$ | $\Delta T_{sol}$ | $T_{lum}$ (20 °C) | $T_{lum}$ (90 °C) | $\Delta T_{lum}$ (20 °C) | $T_{IR}$ (20 °C) | $T_{IR}$ (90 °C) | $\Delta T_{IR}$ (90 °C) | $T_{sol}$ (20 °C) | $T_{sol}$ (90 °C) |
|---|---|---|---|---|---|---|---|---|---|---|
| 230 | 40.1 | 15.0 | 40.1 | 40.1 | 0.1 | 63.3 | 30.9 | 32.4 | 47.5 | 32.5 |
| 55 | 43.3 | 14.9 | 44.4 | 42.2 | 2.2 | 64.0 | 32.2 | 29.8 | 48.9 | 34.0 |

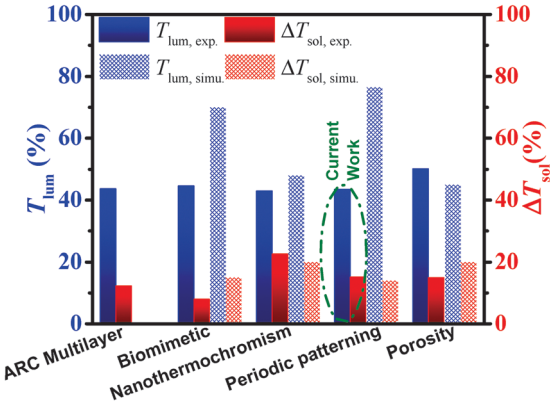


Fig. 5 Current work compared with other best performing samples obtained from different approaches to enhance $VO_2$ performance.[30]

performance compared to continuous samples. The best results obtained were with 0.5 wt% and 0.25 wt% solutions. From the tabulated results (Table 1), the best combination of $T_{lum}$ and $\Delta T_{sol}$ is 43.3% and 14.9%, respectively. As shown in Fig. 5, this result is comparable to some of the best reported porous[33] and antireflective multilayered structure results,[35] and is significantly higher than that of biomimetic moth eyed $VO_2$.[28] Compared with the theoretical results of nano-gridded $VO_2$,[31] the current work can still improve its performance by further reducing its mesh periodicity.

Furthermore, two samples prepared with 0.5 wt% and 0.25 wt% dispersions were tested for their cycling stability. Samples were cycled between 20 °C and 90 °C using an oven for 40 cycles. The UV-Vis-NIR results (Fig. S3, ESI†) show stable performance in terms of $T_{lum}$ and $\Delta T_{sol}$.

## Conclusion

In this report, a simple mesh printing method is employed to produce micro-patterned $VO_2$ films with different periodicities. Compared with continuous nanocomposite film samples, such a structure could enhance $T_{lum}$ due to the opening of the grid, and enables the formation of thicker samples that better capitalize on the additional $VO_2$ content for better $\Delta T_{sol}$. Compared with theoretical work based on a gridded thin film structure, this experimental work can achieve a $\Delta T_{sol}$ as high as 17.2%, which exceeds the calculated $\Delta T_{sol}$ of 16.5%, and an even higher $T_{lum}$ (experimental 21.4% *versus* theoretical 10.5%). This is mainly due to the integration of a gridded structure and nanocomposite $VO_2$. The best performing sample gives 43.3% $T_{lum}$ and 14.9% $\Delta T_{sol}$, which are comparable to most approaches used to enhance thermochromic properties. The facile fabrication method and novel micro-patterned structures open a new and promising direction of $VO_2$ thermochromic materials for smart window applications.

## Acknowledgements

This research was supported by the Singapore National Research Foundation under the CREATE programme: Nanomaterials for Energy and Water Management and Singapore Ministry of Education (MOE) Academic Research Fund Tier 1 RG101/13. XRD, FESEM and TEM characterization was performed at the Facility for Analysis, Characterization, Testing and Simulation (FACTS) in Nanyang Technological University. The first author Lu Qi thanks the financial report from the NTU-JTC Industrial Infrastructure Innovation Centre.

## References

1 R. C. Retzlaff, *J. Am. Plann. Assoc.*, 2008, **74**, 505–519.
2 L. Pérez-Lombard, J. Ortiz and C. Pout, *Energy Build.*, 2008, **40**, 394–398.
3 C. M. Lampert and C. G. Granqvist, *Large-area chromogenics: Materials and devices for transmittance control*, SPIE-The International Society for Optical Engineering, Bellingham, WA, USA, 1990, vol. IS 4.
4 C. Liu, X. Cao, A. Kamyshny, J. Law, S. Magdassi and Y. Long, *J. Colloid Interface Sci.*, 2014, **427**, 49–53.
5 Z. Zhang, Y. Gao, Z. Chen, J. Du, C. Cao, L. Kang and H. Luo, *Langmuir*, 2010, **26**, 10738–10744.
6 A. Cavalleri, C. Tóth, C. W. Siders, J. Squier, F. Ráksi, P. Forget and J. Kieffer, *Phys. Rev. Lett.*, 2001, **87**, 237401.
7 M. M. Qazilbash, M. Brehm, B.-G. Chae, P.-C. Ho, G. O. Andreev, B.-J. Kim, S. J. Yun, A. Balatsky, M. Maple and F. Keilmann, *Science*, 2007, **318**, 1750–1753.
8 F. Morin, *Phys. Rev. Lett.*, 1959, **3**, 34.
9 J. Zhou, Y. Gao, Z. Zhang, H. Luo, C. Cao, Z. Chen, L. Dai and X. Liu, *Sci. Rep.*, 2013, **3**, 3029.
10 N. Wang, S. Liu, X. Zeng, S. Magdassi and Y. Long, *J. Mater. Chem. C*, 2015, **3**, 6771–6777.
11 S. Wang, M. Liu, L. Kong, Y. Long, X. Jiang and A. Yu, *Prog. Mater. Sci.*, 2016, **81**, 1–54.
12 N. Mlyuka, G. Niklasson and C.-G. Granqvist, *Appl. Phys. Lett.*, 2009, **95**, 171909.
13 C.-G. Granqvist, P. Lansåker, N. Mlyuka, G. Niklasson and E. Avendano, *Sol. Energy Mater. Sol. Cells*, 2009, **93**, 2032–2039.
14 S. Chen, L. Dai, J. Liu, Y. Gao, X. Liu, Z. Chen, J. Zhou, C. Cao, P. Han and H. Luo, *Phys. Chem. Chem. Phys.*, 2013, **15**, 17537–17543.
15 C. B. Greenberg, *Thin Solid Films*, 1983, **110**, 73–82.

16 W.-L. Hu, G. Xu, J.-W. Ma, B. Xiong and J.-F. Shi, *Acta Phys.-Chim. Sin.*, 2012, **28**, 1533–1538.
17 N. Wang, M. Duchamp, R. E. Dunin-Borkowski, S. Liu, X. Zeng, X. Cao and Y. Long, *Langmuir*, 2016, **32**, 759–764.
18 X. Cao, N. Wang, S. Magdassi, D. Mandler and Y. Long, *Sci. Adv. Mater.*, 2014, **6**, 558–561.
19 Z. Zhang, Y. Gao, H. Luo, L. Kang, Z. Chen, J. Du, M. Kanehira, Y. Zhang and Z. L. Wang, *Energy Environ. Sci.*, 2011, **4**, 4290–4297.
20 M. Zhou, J. Bao, M. Tao, R. Zhu, Y. Lin, X. Zhang and Y. Xie, *Chem. Commun.*, 2013, **49**, 6021–6023.
21 S. Ding, Z. Liu, D. Li, W. Zhao, Y. Wang, D. Wan and F. Huang, *ACS Appl. Mater. Interfaces*, 2013, **5**, 1630–1635.
22 L. Zhao, L. Miao, C. Liu, C. Li, T. Asaka, Y. Kang, Y. Iwamoto, S. Tanemura, H. Gu and H. Su, *Sci. Rep.*, 2014, **4**, 7000.
23 Z. Chen, C. Cao, S. Chen, H. Luo and Y. Gao, *J. Mater. Chem. A*, 2014, **2**, 11874–11884.
24 J. Du, Y. Gao, H. Luo, Z. Zhang, L. Kang and Z. Chen, *Sol. Energy Mater. Sol. Cells*, 2011, **95**, 1604–1609.
25 S.-Y. Li, G. A. Niklasson and C.-G. Granqvist, *Appl. Phys. Lett.*, 2011, **99**, 131907.
26 Y. Gao, S. Wang, L. Kang, Z. Chen, J. Du, X. Liu, H. Luo and M. Kanehira, *Energy Environ. Sci.*, 2012, **5**, 8234–8237.
27 X. Qian, N. Wang, Y. Li, J. Zhang, Z. Xu and Y. Long, *Langmuir*, 2014, **30**, 10766–10771.
28 A. Taylor, I. Parkin, N. Noor, C. Tummeltshammer, M. S. Brown and I. Papakonstantinou, *Opt. Express*, 2013, **21**, A750–A764.
29 Y. Zhou, Y. Cai, X. Hu and Y. Long, *J. Mater. Chem. A*, 2014, **2**, 13550–13555.
30 Y. Zhou, Y. Cai, X. Hu and Y. Long, *J. Mater. Chem. A*, 2015, **3**, 1121–1126.
31 C. Liu, I. Balin, S. Magdassi, I. Abdulhalim and Y. Long, *Opt. Express*, 2015, **23**, A124–A132.
32 S.-Y. Li, G. A. Niklasson and C.-G. Granqvist, *J. Appl. Phys.*, 2010, **108**, 063525.
33 L. Kang, Y. Gao, H. Luo, Z. Chen, J. Du and Z. Zhang, *ACS Appl. Mater. Interfaces*, 2011, **3**, 135–138.
34 M. Layani and S. Magdassi, *J. Mater. Chem.*, 2011, **21**, 15378–15382.
35 N. R. Mlyuka, G. A. Niklasson and C. G. Granqvist, *Phys. Status Solidi A*, 2009, **206**, 2155–2160.
36 G. Wyszecki and W. S. Stiles, *Color Science: Concepts and Methods, Quantitative Data and Fomulae*, Wiley, New York, 2nd edn, 2000.
37 In ASTM G173-03 Standard Tables of Reference Solar Spectral Irradiances: Direct Normal and Hemispherical on a 37° Tilted Surface, Annual Book of ASTM Standards American Society for Testing and Materials, Philadelphia, PA, USA, 2003, vol. 14.04, http://rredc.nrel.gov/solar/spectra/am1.5.